Computers in Biology and Medicine 39 (2009) 978–988

Contents lists available at ScienceDirect

Computers in Biology and Medicine

journal homepage: www.elsevier.com/locate/cbm

Gaussian source model based iterative algorithm for EEG source imaging

Xu Lei[a], Peng Xu[a], Antao Chen[a,b], Dezhong Yao[a,*]

[a]Key Laboratory for NeuroInformation of Ministry of Education, School of Life Science and Technology, University of Electronic Science and Technology of China, Chengdu 610054, China
[b]Key Laboratory of Cognition and Personality of MOE, Southwest University, Chongqing 400715, China

ARTICLE INFO

Article history:
Received 19 February 2009
Accepted 24 July 2009

Keywords:
EEG source imaging
Gaussian source model
Underdetermined system
FOCUSS
Inverse problem

ABSTRACT

Estimation of the neural active sources from the scalp electroencephalogram (EEG) is an ill-posed inverse problem. In this paper, we propose a new source model: Gaussian distributed Source Model (GSM), to model the activations in brain. GSM may imitate an Isolated Source Model (ISM) or a Distributed Source Model (DSM) by adopting different supporting range parameter of the Gaussian function. Using GSM, an iterative Gaussian source Imaging Algorithm (GIA) is developed to detect the EEG sources. As GIA dynamically reduces the solution space, the solution may gradually converge to a desired distribution. A comparative evaluation among LORETA, FOCUSS and GIA was conducted for both isolated point sources and distributed sources, the results demonstrate that GIA is more flexible and efficient for various actual sources configurations. Finally, GSM was applied to real recordings obtained from a visual spatial attention task; the corresponding source activation areas of the early component are localized in contralateral occipital cortices, consistent with the retinotopic organization of early visual spatial attention effects.

1. Introduction

The scalp electroencephalogram (EEG) represents electrical activity manifested by the ensemble of a great number of neurons within the brain. When a large number of neurons synchronously change their post-synaptic potentials, significant currents start to flow in the surrounding tissue and they may produce potentials at a level that is possibly to be recorded by electrodes on the scalp. Currently, the pyramidal neurons of layer IV, aligned in parallel and widely inter-connected, are thought to be one of the main cells responsible for scalp EEG potentials [1], and deeper cortical structures including hippocampus, cerebellum and thalamus may potentially contribute to EEG, too [2]. A set of active pyramidal cells can be modeled electrically as a dipole layer [3].

Estimating the location and distribution of the underlying neural generators based on the scalp EEG is a typical inverse problem, and it greatly depends on the source model selected [4]. If one assumes that only a few restricted areas are active simultaneously and each area evolves with a unified temporal process, then the EEG potentials can be modeled by a small set of isolated dipoles, the Isolated point Source Model (ISM). This localized single time-course hypothesis is both convenient and fairly realistic since neurons in a population are expected to be strongly coherent in time [5]. However, ISM has some drawbacks to be tackled. ISM position may well approximate the center of a cortical patch, yet it is not able to describe its extent. Indeed, in case of a highly extended cortical area, even the optimal ISM localization may be meaningless [6]. Worse more, in the case of multiple sources, estimating the number of dipoles is often a difficult task [7]. These potential traps have led some scientists to prefer distributed sources where a large number of dipoles are placed evenly in the head, either in the whole brain volume [8] or along the surface of the cortex [9], the Distributed Source Model (DSM). Usually, additional spatial and/or temporal constraints are used to reduce the under-determination of DSM inverse solution [10]. The current constraints include minimum norm (MN) [8], maximum spatial smoothness [11], sparsity [12,13] or Bayesian approaches [14,15] and these constraints are partly reasonable in sense of the actual neurophysiology.

In this work, we are going to seek if there is a further constraint for DSM that is physiologically reasonable and meaningful for improving the neural source imaging. Based on some neurophysiological facts, we assume the equivalent dipoles in a restricted area will be approximately oriented in the same direction, and their strengths are close to a Gaussian distribution. Apparently, such a Gaussian distributed Source Model (GSM) is consisted of a group of sources closely located, and it is determined by the center of the "group" and the support range of the Gaussian distribution. Most importantly, GSM may flexibly cover the conventional ISM and DSM by using a narrow or wide support range of the Gaussian distribution. The detail of GSM is introduced in Section 2, then a corresponding algorithm, Gaussian source Imaging Algorithm (GIA), is introduced in Section 3, and the adopted head model and evaluation indexes were given in Section 4

* Corresponding author. Tel.: +86 28 83201018; fax: +86 28 83208238.
E-mail address: dyao@uestc.edu.cn (D. Yao).

0010-4825/$ - see front matter © 2009 Published by Elsevier Ltd.
doi:10.1016/j.compbiomed.2009.07.012

GIA is tested and compared with LORETA [11], the improved FOCUSS algorithm [16] under various noisy situations in Section 5. In Section 6, GSM was applied to real recordings. Finally, discussions and conclusions are given in Section 7, respectively.

2. Methods

2.1. Isolated point source model

In ISM, no matter dipole or charge [17,18], sources are assumed to be located at a few distinct positions. Under the assumption of a few isolated point sources, the sources can be uniquely identified mathematically [19] and the parameters may be estimated by various nonlinear optimization algorithms [20].

The advantage of ISM is its simplicity and the main drawback is that one needs to priori specify the number of sources, which is unfeasible for many problems [7]. Furthermore, the optimization is often trapped in the local minima and the sources to be localized need to be of small number. In addition, as some researches revealed, for complex cognitive processes or widespread epileptic discharges, the ISM assumption is inappropriate [7].

2.2. Distributed source model

In DSM [8,21,22], the number of unknown variables is usually much larger than the number of measurement electrodes, some additional constraints on the solution are needed, such as minimum norm (MN) [8] or smooth requirement in low resolution electromagnetic tomography (LORETA) [11]. The result of LORETA is very blurring, and the current neurophysiological functional localization idea indicates that the main neural electric activities should be sparsely localized [13,22], thus a reasonable solution should not only explain the scalp recordings but also be sparsely localized. Presently, there are two approaches to get sparse solution. One way is to directly solve the l_p ($p \leq 1$) norm solution, such as the l_1 norm solution [13]. Another way is to shrink the solution space iteratively thus to change the initially underdetermined problem to a finally overdetermined problem. In this approach, an initial blurring distributed source solution, such as LORETA, is obtained firstly, then with iteratively shrinking the solution space, the solution gradually converges to a relatively sparse one, such as the focal underdetermined system solver (FOCUSS) [12,23] and the self-coherence enhancement algorithm (SCEA) [21].

2.3. Gaussian source model

As shown above, both ISM and DSM have their own advantages and disadvantages, and the tricking point is quite possibly the "isolated" (ISM) or "distributed" (DSM) requirement. In fact, in our previous work of scalp Laplacian [24], we found that a Gaussian radial-basis function (RBF) based Laplacian is better than the previous local or global Laplacian, and the reason is that the Gauss function with the flexible support range in space provides a choice over local or the global approaches. Now, for the EEG inverse problem, is there a better source model integrating the advantages of ISM and DSM? We believe that GSM is one of the answers. Neurophysiologically, cortical neurons are known to be strongly interconnected and aligned in parallel [1]. The scalp potential is thought to be generated by synchronized post-synaptic activity of neuronal macrocolumns [6]. The macrocolumns that with common functional properties are grouped together [25] and their preferred stimulus values progress gradually across the cortical sheet [26]. In addition, cortical activation always propagates into the adjacent regions very soon [27]. These facts mean the focally clustered dipoles have parallel orientation and gradualness distribution. Hence such a distributed source is a situation from the very locally equivalent point source to the extreme uniform distribution source, Gaussian distribution would be a more adaptive and flexible approximation compared to these two existed distributions. On the other hand, Gaussian distribution with adaptive shape can evolve to any one of these two cases when necessary.

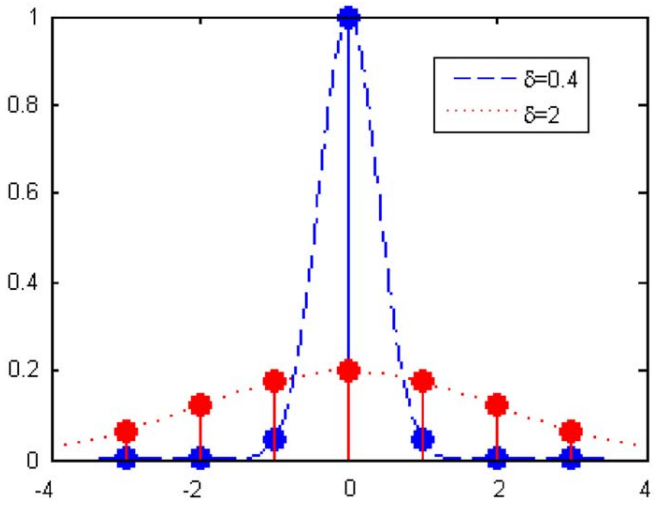

Fig. 1. Gaussian function with different standard deviation σ. Blue bashed line: $\sigma = 0.4$ and red dotted line: $\sigma = 2$. (For interpretation of the references to color in this figure legend, the reader is referred to the web version of this article.)

Based on the above facts, we assume the neural electric sources of the scalp recordings are in Gaussian distribution for each restricted active area, thus their spatial extent may be approximately described by Gaussian function. With GSM, there may have a few restricted areas being simultaneously activated, and for each area, the neighboring neurons are aligned in parallel [1], and their strengths are in Gaussian distribution:

$$\varphi(z,\sigma) = \frac{1}{\sigma\sqrt{2\pi}} \exp\left(-\frac{z^2}{2\sigma^2}\right), \tag{1}$$

where z denote the variable and σ is the standard deviation, which determines the support range. Fig. 1 shows two Gaussian functions with different standard deviations. Obviously, with the larger $\sigma = 2$, the half-strength distributed sources are from grid -3 to 3; with the smaller $\sigma = 0.4$, only a point source located at grid 0 is remained. These facts mean that, with GSM, DSM and ISM can be easily realized, thus even GSM is not a strict model of the real neural electric source, it provides more general adaptation for various practical problems than the previous DSM and ISM.

2.4. Linear inversion problem and LORETA

Based on DSM, EEG inverse problem can be stated as

$$Y = AX + E, \tag{2}$$

where Y is the scalp recordings of $M\times1$, M is the number of electrodes. A is the lead field matrix of $M\times3N$, where N is the size of the solution space, 3 indicates the three orthogonal components of each dipole. X is the source solution matrix of $3N\times1$, consisted of N column vectors of size 3×1, $X(j)$ for each grid node in solution space, $j = 1,\ldots,N$. E is the noise vector in the recordings. Here M is usually much smaller than N. Eq. (2) is a linear equation, and the EEG inverse problem is to solve this equation. In LORETA [11,18], the solution is

$$X = W^{-1}A^T[AW^{-1}A^T]^+Y, \tag{3}$$

where $[\,]^+$ denotes the Moore–Penrose pseudo-inverse. The weighted matrix W is defined as

$$W = B \times diag(\|A_1\|, \|A_2\|, \ldots, \|A_{3N}\|), \tag{4}$$

where B denotes the discrete spatial Laplacian operator; $\|A_i\|$ is the ith column norm of the lead field matrix A.

2.5. FOCUSS

FOCUSS is an energy localized iterative procedure [12,23]. By a linear transform $X = Wq$, Eq. (2) is changed to

$$\begin{cases} \min & ||q|| \\ \text{s.t.}: & AWq = Y. \end{cases} \tag{5}$$

FOCUSS is an iterative procedure and in its kth iteration the transform W_k is a diagonal matrix constructed by the prior iteration solution X_{k-1}. The iteration procedure can be briefly stated as the following two steps:

$$(1)\quad W_k = Diag[1/\|A_1\|, \ldots, 1/\|A_{3N}\|] \times (Diag(X_{k-1})), \tag{6}$$

$$(2)\quad X_k = W_k W_k^T A^T (A W_k W^T A^T)^+ Y, \tag{7}$$

where $\|A_i\|$ is the norm of the ith column of the matrix A. W_k is constructed directly from the amplitudes of the elements of X_{k-1} estimated in the preceding steps, which in turn enhances some of the elements in X_{k-1} having large amplitude. As FOCUSS tends to enhance those prominent solution elements with relatively large amplitude and simultaneously decrease the remaining elements until they become zero during iteration procedure, a proper initialization is important for correct localization when FOCUSS is used. The smooth source distribution provided by LORETA is the widely accepted choice in current practice. In each step of the current FOCUSS, the solution space is the same, $3N$ in our model. The algorithm must, therefore, repeatedly handle large matrices, even though many elements in the solution are forced toward zero during the iteration procedure. Moreover, there is nothing inherent in the methodology to limit an increase in error from the current iteration to the next. And if some real sources are incorrectly eliminated at some previous steps, it is hard to recover them in the subsequent iterations [22].

2.6. GIA

In GSM, we assume the sources in a local area are approximately of same orientation with strengths in Gaussian distribution. Combining GSM with the iterative strategy of FOCUSS, we have a new algorithm-GSM based Iterative Algorithm (GIA), which can be realized with the following steps:

(1) *Initialization*: Iteration index $k = 1$; the maximum iteration number $T_{\max}$ and the tolerances error ξ to terminate the iteration; initialize source distribution X_0 with LORETA solution; initialize neighboring range d_1 for searching a local peak in X_0.
(2) Solve Eqs. (6) and (7) for X_k.
(3) *GSM process*: Determine the parameters of GSMs as follows.
   (i) *GSM center*: Each GSM center is defined as the grid node which meets the following two conditions: (a) its magnitude P (a scalar term) is larger than 1% of the maximum value in the entire solution space and (b) P is the largest one among the nearest six neighbors (for boundary nodes, the number of the nearest neighbors may be smaller than 6).
   (ii) *GSM neighbors*: Neighbors of each GSM consist of these nodes within the sphere located at the center of this GSM with radius d_k.
   (iii) *Adjust the source at each GSM neighbor*: The source strength is re-determined by the Gaussian function. For such as the ith GSM, firstly, its σ_i is determined, and then, the dipole moment is readjusted. σ_i is defined by the local maximum $P_{\max}$ and the mean value of its nearest neighbors $P_{neighbor}$:

$$\sigma_i^2 = D^2/\ln(P_{\max}/P_{neighbor}), \tag{8}$$

   where D is the distance between the local maximum and its nearest neighbor, the inter-grid distance. The dipole moment of a neighbor node noted by position vector s_j is determined by

$$Q_j = Q_i \times \exp\left(-\frac{\|s_i - s_j\|^2}{\sigma_i^2}\right). \tag{9}$$

   The Q_i denotes the dipole moment of the center node i, its magnitude is the local maximum $P_{\max}$. The s_i and s_j are the spatial position vectors of the grid nodes i and j, respectively. If P_j, norm of Q_j is larger than that of the current solution at node j, norm of $X_k(j)$, Q_j is set to node j. Otherwise, moment of node j will not be changed.
(4) *Solution space shrinking*: Redefine the solution space to include only the nodes covered by GSMs. i.e., only keep the corresponding elements in X and columns in A. The size of matrix X and A will, thus, decrease with subsequent iterations. After each iteration, take the new A for Eqs. (2), (5)–(7), and set $d_{k+1} = d_k/2$.
(5) *Termination judgment*: $k = k+1$, repeat steps (2), (3) and (4) until a stopping condition initialized in step (1) is satisfied, as discussed below.
(6) *GIA solution*: Let the solution of the last iteration be the GIA solution.

Note that steps (3) and (4) are the smoothing and shrinking operations that modify the solution space. In our practice, we stop changing the solution space when any of the following conditions are met: (1) The new solution space has fewer nodes than the number of sensors; (2) the difference between the current and the last solution is smaller than the iteration termination error ξ, i.e., $\|X_k - X_{k-1}\| < \xi$; and (3) the iteration step is larger than the max iteration ($k > T_{\max}$). The first condition implies that the shrinking operation has turned the under-determined problem into an over-determined problem. The second condition indicates the solution has converged. In either case, we stop the shrinking and smoothing operations and repeat only step (2) until convergence. Step (2) transforms the procedure into a FOCUSS process and it is guaranteed to converge as shown in reference [23]. Detailed discussion about convergence is given in Section 4.

2.7. Head model

As shown in Fig. 2, simulations were conducted on a standard 3-shell realistic head model registered to Talairach human brain atlas [28]. The conductivities for brain tissue cortex, skull and scalp are 1.0, 0.0125, and $1.0\,\Omega^{-1}\,m^{-1}$, respectively. The solution space is restricted to cortical gray matter and hippocampus, consisting of 6777 nodes at 5-mm spatial resolution. The lead field matrix calculated with dipole model by boundary element method (BEM) is of 129×20 331, where 20 331 = 6777×3. The origin of the coordinate system is defined as the midpoint between the left and right preauriculars, and the directed line from the origin through the nasion defines the +X-axis, the +Y-axis is the directed line from the origin through the left preauricular. Finally, the +Z-axis is the line from the

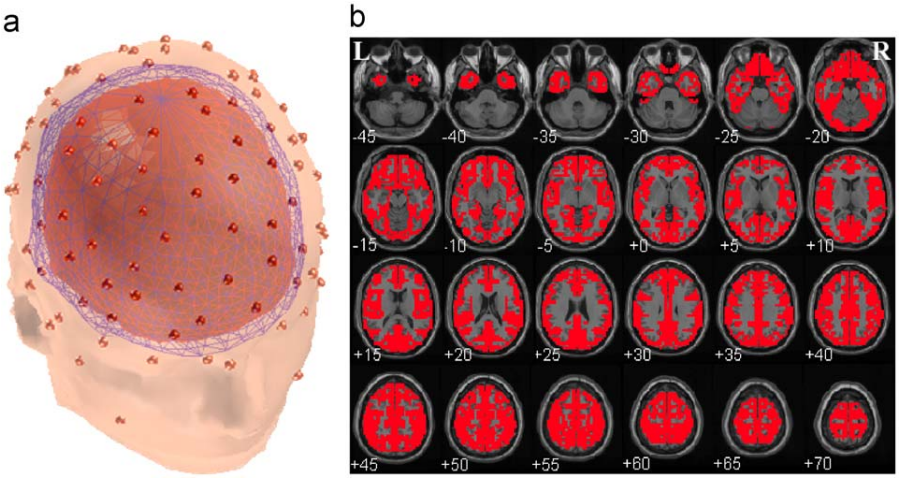

Fig. 2. The 3-shell realistic head model and solution space used to define the forward model: (a) the three meshes correspond to the scalp, the skull and cortex. The red dots indicate the position of the 129 EEG channels and 3 EOG channels. Channel locations were registered to the scalp meshes and (b) solution space of the inverse problem. The upper-left slice is the lowest part of the brain; the lower-right slice is the topmost part of the brain. (For interpretation of the references to color in this figure legend, the reader is referred to the web version of this article.)

origin toward the top of the head (through electrode Cz). The 129 electrodes were registered on the scalp.

2.8. Evaluation indexes

In this work, we take the following three evaluation indexes. One is the localization error [4], $E_{localization}$, which is the distance between the simulated and the estimated point source, the center of DSM, respectively, the estimated one is automatically searched within a spherical volume with radius r_e centered at the assumed one; the second is the source energy error [4], $E_{energy} = \|X_{est} - X_{\max}\|/\|X_{est}\|$, which is used to measure the source energy recovery ability, where $X_{\max}$ is the moment of the simulated point source or the moment at the center of DSM, X_{est} is the moment of the estimated source with maximum power within a spherical volume with radius r_e centered at the simulated one. The third is the normalized blurring index (NBI) in region of interest (ROI) to measure the spatial resolution ability [21], $NBI_i = \sqrt{\sum_l \|r_l - r_i\|^2 X^2(l)/\sum_l X^2(l)}/\sqrt{\sum_l \|r_l - r_i\|^2/\sum_l 1}$, where the subscript i refers to a grid node of the solution space in the 3-D model, for assumed point source, it is selected as the actual node position of the simulated point dipole, for the assumed DSM, it is the center node. For the reconstructed distributions, it is selected as the node with maximum power within a spherical volume with radius r_e centered at the simulated one. The subscript l refers to the neighboring nodes within the spherical ROI with radius r_n centered at the node i, and $\sum_l 1$ is the total nodes in this ROI. $X(l)$ is the moment value at node l, s_l and s_i are the spatial position vectors corresponding to the grid nodes l and i, respectively. Generally, the smoother the sources in ROI are the closer to 1 the NBI is; otherwise, if the sources are sharply distributed, NBI is close to 0. Obviously, for well isolated sources, a small NBI is expected. An excellent localization algorithm should be of low $E_{localization}$, E_{energy}, and a NBI similar to the NBI of the actual source.

In this paper, the noise-to-signal-ratio (NSR) is defined as the ratio between the power of noise and that of signal. In all the simulations, the maximum iteration number was 10 for FOCUSS and 6 for GIA.

3. Results

3.1. Tests for isolated point source

In this simulation, we evaluate the efficiency of LORETA, FOCUSS and GIA when applied to localize three isolated sources. Three dipole sources with moments of (2.64, 6.60, −5.28), (1.78, 8.91, −1.78) and (−6.11, 3.82, −7.64) were placed at three isolated positions (10, 25, −20), (−15, −75, 15) and (40, −25, 50) (mm), respectively. The scalp potentials were obtained by BEM and contaminated with Gaussian noise of different *NSR*s. For different NSR cases, LORETA, FOCUSS, and GIA were taken for source imaging. The $E_{localization}$ and E_{energy} were calculated with $r_e = 25$ mm. For NBI, $r_n = 25$ mm and the center for calculation is at the position of the estimated source with the maximum power. The localization results were shown on the MRI slices in Fig. 3 and the performances in all noise cases were shown in Fig. 4.

As shown in Figs. 3 and 4, among these three localization algorithms, the estimated sources areas with LORETA were mostly blurring, usually large clouds on the MRI slices, and the $E_{localization}$, E_{energy}, and *NBI* of LORETA were relatively large when compared with the other two methods. While in all simulated cases, LORETA could establish a relatively strong source at the corresponding simulated source position like that with $NSR = 0.15$ shown in Fig. 4. For FOCUSS, when $NSR < 0.05$, the $E_{localization}$, E_{energy}, and NBI were small, which meant that the localization ability of FOCUSS under low NSR was good for isolated sparse sources. But for $NSR > 0.05$, FOCUSS was not stable with a remarkable increase of $E_{localization}$, E_{energy}. As shown by Fig. 4 for $NSR = 0.15$, no strong sources were obtained by FOCUSS at the assumed source positions, even some far away fake weak sources were generated. For GIA, in all the cases, the $E_{localization}$ was nearly 0.0. Comparing GIA with FOCUSS (Fig. 4), the sources configuration localized by GIA was much clearer and of fewer fake sources. The E_{energy} and *NBI*s of GIA were also relatively small. All the three indexes showed that GIA was much stabler over noise than FOCUSS.

Furthermore, the statistical performances of these three algorithms were evaluated by a way similar to the Mont Carlo simulation. As the literature [13,22] described, by placing one dipole source on each grid node (totally 100 randomly selected nodes) of the solution space, $E_{localization}$ and E_{energy} were calculated for each grid node, and then the mean and standard deviation (SD) of $E_{localization}$ and E_{energy} were calculated, respectively. For each of the 100 positions, a dipole with moment randomly selected within [−5, 5] was put on it. And for each case, the simulated scalp data was mixed with $NSR = 0.1$. $E_{localization}$ and E_{energy} were calculated between the simulated one and the estimated source with maximum power, and *NBI* was calculated at the position of the estimated source with maximum power.

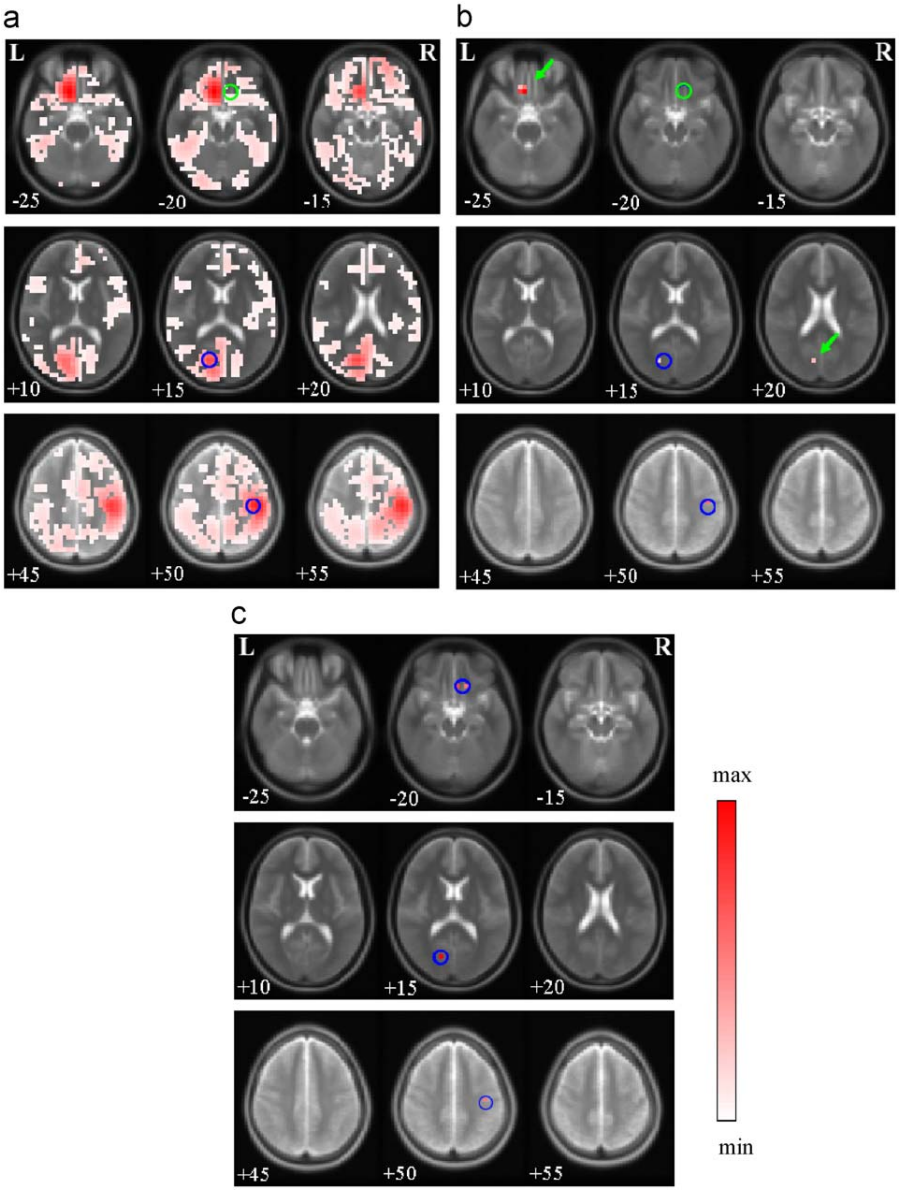

Fig. 3. Localization results of LORETA, FOCUSS and GIA on MRI slices at the simulated source positions for three isolated sources under noise of $NSR = 0.15$: (a) LORETA, the nodes with power smaller than 1% of the maximum value in the entire brain volume are discarded; (b) FOCUSS localized sources; (c) GIA localized sources. Colorful rectangle area is the estimated source location; the center of circle is the simulated source. Blue circle around the colorful rectangle area indicates the overlapping area of the simulated source and the estimated source; green circle indicates those simulated source locations that are not overlapped with the positions of the estimated sources; green arrow indicates those estimated sources locations near the simulated sources. In LORETA results (a) and FOCUSS results (b), no corresponding sources at the position of simulated deep source 1 were found. (For interpretation of the references to color in this figure legend, the reader is referred to the web version of this article.)

The mean and SD of the three evaluation indexes for the 100 cases were shown in Fig. 5. As the results show, LORETA has the largest $E_{localization}$, E_{energy} and *NBI*, GIA has the smallest $E_{localization}$, and *NBI* of GIA is smaller than LORETA, but larger than FOCUSS. That is to say, the isolated point-like source can be robustly localized by GIA with an acceptable distance and energy error. While, due to the smoothing effect of GSM, the solution of GSM is a little smoother than FOCUSS, but it is much more regional than LORETA.

3.2. Test for extended sources

In this section, the results for two focally distributed sources were shown. One DSM with 27 dipoles were placed within a sphere centered at $(-15, -75, 15)$ (mm) with radius of $5\sqrt{3}$ mm, the dipole moment was set according to a Gaussian distribution with $\sigma = 11.7$. Another DSM with seven dipoles were placed within a sphere centered at $(60, -25, 35)$ (mm) with radius of 5 mm. The dipole moment was the same within this sphere. They were listed in Table 1 ($NSR = 0.1$).

The above three indexes for these focally extended sources were calculated as follows. The central of the simulated DSM was taken as the reference node. $E_{localization}$ was the distance between the reference and the node with the maximum power in the estimated sources. *NBI*s were calculated with r_n=30 mm-sphere centered at the central positions of the simulated or the estimated dipoles with maximum powers, respectively. E_{energy} was the average obtained over all the simulated or estimated sources, respectively. The results on MRI

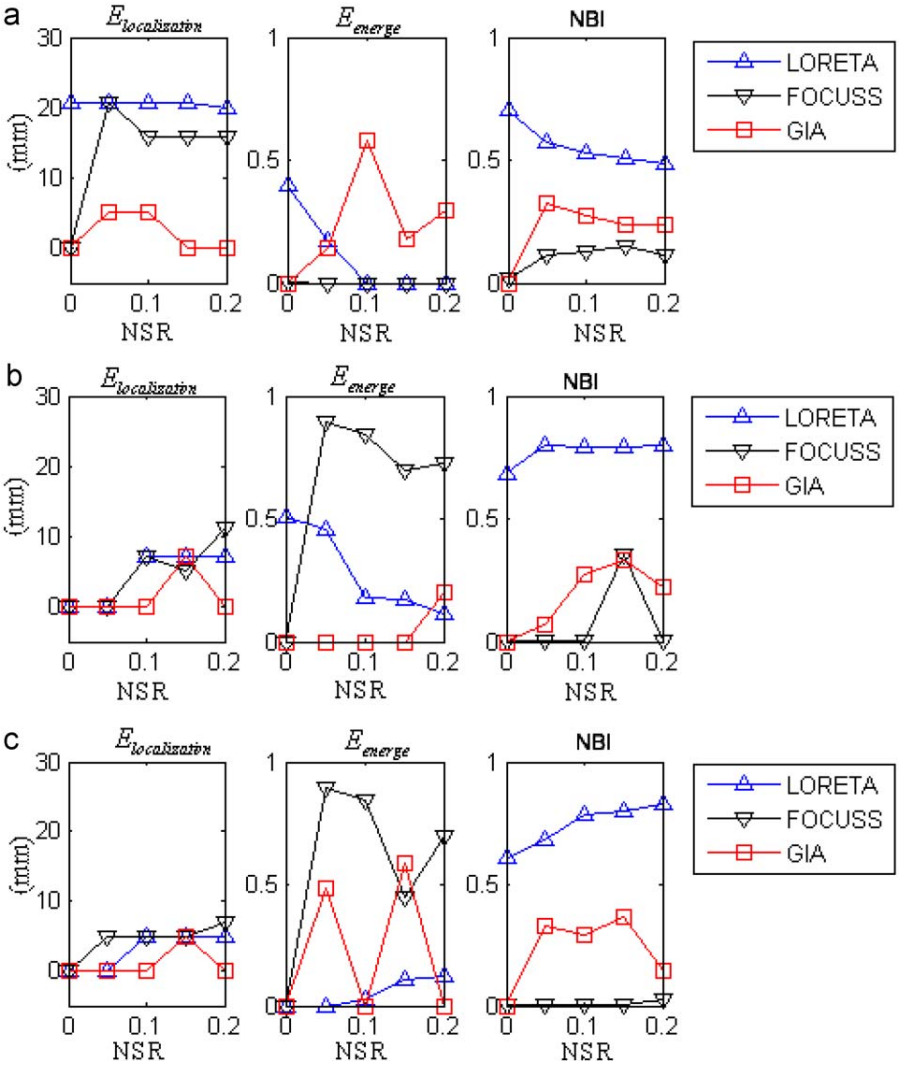

Fig. 4. Localization indexes at different noise *NSRs*: (a) Source 1; (b) Source 2; and (c) Source 3.

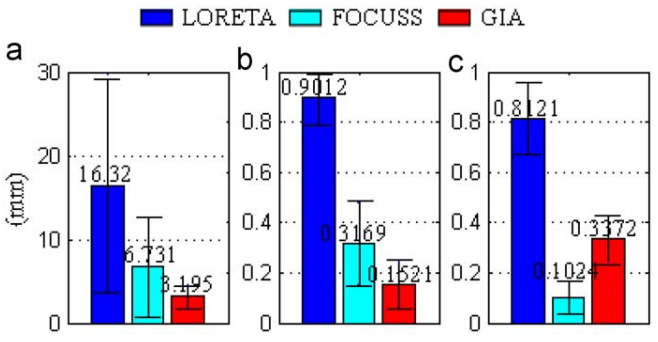

Fig. 5. Statistical features of the three methods: (a) mean and SD of $E_{localization}$; (b) mean and SD of E_{energe}; and (c) mean and SD of *NBI*.

slices near the simulated sources area were shown in Fig. 6 and the indexes were listed in Table 2, too.

On the MRI slices, the estimated sources area by LORETA (FOCUSS) was much broader (smaller) than actually it was, and that of GIA was similar to the true case. The nodes number with power larger than 50% of the maximum in the entire brain volume was 152 for LORETA, 17 for FOCUSS and 33 for GIA, respectively. For the assumed DSM source with Gaussian distribution, the $E_{localization}$ and E_{energy} of GIA were 0.3208 and 0.3121 mm, respectively, and they were the smallest among the three methods. The NBI of GIA was 0.9613, the closest to the actual NBI (0.9339). These facts mean that, GIA perfectly reconstructed this DSM with Gaussian distribution. For the assumed DSM source, the $E_{localization}$ and E_{energy} of GIA were 0.0 and 0.0191, respectively, and they were the smallest among the three methods, too. The NBI of GIA was 0.9800, a similar value of LORETA (0.9825), and they are close to the actual 1.000. However, by FOCUSS, only one node is found, and its NBI (0) is far away from the actual one. These facts mean that, with the emphasis on the sparsity of the extended source, FOCUSS may converge to an over-sparser solution with fewer dipoles. Apparently, FOCUSS is not suitable for DSM, and GIA is still meaningful for DSM.

The ideal case is that all the simulated distributed source be recovered correctly, it is rather difficult for EEG inverse problem, and generally if most of the estimated sources are located near or within the simulated area and the difference of NBI between the simulated distributed source and the estimated distributed source is not too large, the localization could be thought to be successful for the

Table 1
Moment and position of each dipole.

Source	Moments	Positions [x, y, z] (mm)
Gaussian distribution	[−1.1547 −5.7735 1.1547]	Center of source 1: [−15, −75, 15]
	[−0.9623 −4.8113 0.9623]	[−15 −75 10] [−20 −75 15] [−15 −80 15] [−15 −70 15] [−10 −75 15] [−15 −75 20]
	[−0.8019 −4.0094 0.8019]	[−20 −75 10] [−15 −80 10] [−15 −70 10] [−10 −75 10] [−20 −80 15] [−20 −70 15] [−10 −80 15] [−10 −70 15] [−20 −75 20] [−15 −80 20] [−15 −70 20] [−10 −75 20]
	[−0.6682 −3.3411 0.6682]	[−20 −80 10] [−20 −70 10] [−10 −80 10] [−10 −70 10] [−20 −80 20] [−20 −70 20] [−10 −80 20] [−10 −70 20]
Uniform distribution	[4.0637 −1.6932 2.3705]	Center of source 2: [60 −25 35] [60 −25 30] [55 −25 35] [60 −30 35] [60 −20 35] [65 −25 35] [60 −25 40]

extended source [10]. By the estimated source locations on MRI slices (Fig. 6) and the indexes in Table 2, all the three methods were successful in this simulation study. Each of them established a corresponding equivalent source distribution, and the differences among them were that the result of LORETA was a blurring and enlarged area, and that of FOCUSS was a little sparse and focal areas, only GIA almost correctly recovered the features of both DSM with Gaussian and uniformly distribution sources. This simulation also showed that different localization method may result in a different equivalent source distribution and the difference should be taken into account in explanation of the result for an EEG inverse problem, especially for the real EEG data [10].

3.3. Real data test

3.3.1. Experiment

Classical experiment paradigm of spatial selective attention was adopted to acquire the ERP recordings [29–31], data were collected in a spatial selective attention study with the NeuroScan System [32]. Ten normal healthy right-handed subjects include seven males and three females, 22–34 years old, were recruited from universities in Beijing. They had no hearing and seeing problems and were paid after testing. The stimulus consists of two different sizes of small circular checkerboards. The bigger checkerboard is the standard stimulus and the smaller one is the target stimulus, with a probability of 80% and 20%, respectively. All stimuli were presented to left or right visual field with a rapid random sequence and each subject was required to focus on one visual field at a time and respond to the targets using a keyboard. The durations of the stimuli were 59 ms and the interstimulus interval (ISI) ranged randomly between 250 and 550 ms. Total 16 blocks were presented, each block consisted of 100 trials and short breaks were allowed between blocks.

The same electrode montage as that used in simulation is adopted to record EEG in this experiment. Considering the signal quality, the recordings are visually inspected and the bad or artifact contaminated channels and the three EOG channels are not involved in the further analysis, and 119 sensors in the 132 sensors are finally used for EEG source estimation. Grand average visual ERPs over ten subjects recorded from 119 scalp sites were analyzed. EEG was digitized at a rate of 250 Hz and average reference was adopted. The electrooculogram (EOG) was recorded, trials contaminated with EOG artifacts (mean EOG voltage exceeding $\pm 80\,\mu V$) or those with artifacts due to amplifier clipping, bursts of electromyographic (EMG) activity, or peak-to-peak deflection exceeding $\pm 80\,\mu V$ were excluded from averaging. Electrode positions (localized by NeuroScan System) are group-averaged over ten subjects. Then positions are coregistrated to our standard 3-shell realistic head model. Attention to the stimulus location produces increased amplitude of the P100 (80–130 ms) component over the contra-occipital scalp [31]. In the present study, the data with attention to the right visual field and stimulus location in the same field (attended data), and the data with attention to the left visual field and stimulus at the right visual field (unattended data) were analyzed in detail.

As shown in Fig. 7, an enlarged P100 component was observed over the hemisphere contralateral to the attended right visual field in O1, which is in line with previous studies [29–31]. P100 shows a significant peak at 96 ms after the onset of the target, and the following analysis is focused on this component.

3.3.2. Result and discussions of attended VEP

For attended case, as shown in Fig. 8, the activations in the bilateral inferior temporal (Brodmann area 20, Fig. 8(a.1)) and fusiform gyrus (Brodmann area 19 Fig. 8(a.2)) were detected by LORETA. However, the active on right calcarine cuneus (Brodmann area 17 Fig. 8 (a.3)) is hard to correlate with certain cognitive function because a stimulus at the right would mainly result in neural activities at the left occipital cortex. FOCUSS localized activations in right inferior occipital (Fig. 8(b.1)) and left fusiform gyrus (Brodmann area 19, Fig. 8 (b.2)). The action on right inferior occipital is also difficult to explain. For GIA (Fig. 8(c)), three activation areas were detected: temporal fusiform gyrus (Brodmann area 19), occipital fusiform gyrus (Brodmann area 37) and middle occipital gyrus (Brodmann area 19). These strong activations all are in the contralateral (left) dorsal occipital areas (Fig. 8(c.1-2)), which are associable with sustained attention and the focal early ERP positivity effect [30]. The effect in the fusiform gyrus (Fig. 8(c.3)) seen in the present experiment may reflect some activation of the ventral pathway for object analysis or other higher-order processing as lateralized attention to right visual stimuli may result in both ventral (fusiform gyrus) and dorsal (middle occipital gyrus). Compared with the other two methods, GIA result is more consistent with previous functional neuroimaging studies [29]. Similar to the simulations, activations detected by LORETA were of large area and the activations localized by FOCUSS and GIA were relatively sparse and local, and the result of GIA seems most meaningful.

3.3.3. Result and discussions of the difference between attended and unattended VEP

The reasonable result of GIA spirit us to analyze the difference data between attended and unattended data in detail. As shown in Fig. 9(a), under condition of unattended, the activations in the bilateral inferior temporal and fusiform gyrus were detected and contrast with the result of attended data (Fig. 8(c)), fewer cortexes is active. More interesting is that, compared to the attended condition, the area coverage is reduced. This is intelligibly as that the spatial attention exerts a gain control or selective amplification of sensory information flow in the visual pathways, thus the involved neural mass may be different for the attended and unattended cases. By GIA, the support range of a neural event may be recovered with dynamical

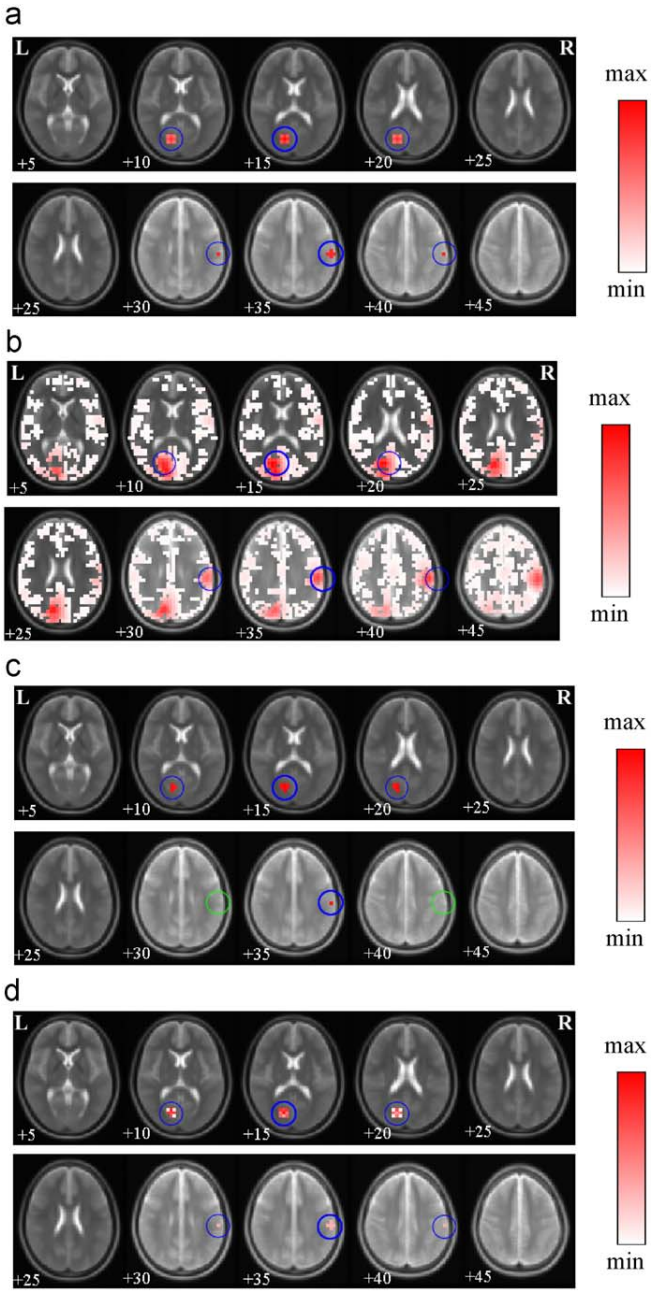

Fig. 6. Localization results of LORETA, FOCUSS, and GIA on MRI slices near the simulated sources area for a focally extended source under noise of $NSR = 0.15$. (a) GSM centered at $(-15, -75, 15)$(mm) with radius of $5\sqrt{3}$ mm, DSM centered at $(60, -25, 35)$(mm) with radius of 5 mm; (b) LORETA; (c) FOCUSS; and (d) GIA. Colorful rectangle area is the estimated source location; the center of circle is the simulated source. Blue circle around the colorful rectangle area indicates the overlapping area of the simulated source and the estimated source; green circle indicates those simulated source locations that are not overlapped with the positions of the estimated sources. (For interpretation of the references to color in this figure legend, the reader is referred to the web version of this article.)

adjustment of $-\sigma$. In Section 4, we will discuss this in more detail.

To verify the exact localization of this early spatial attention effect, the difference data between attended data and unattended data were analyzed to eliminate any nonspecific arousal or motivational effects. As shown in Fig. 9(b), the effect is only localized in the fusiform gyrus. This result is consistent with previous ERP and blood-flow neuroimaging studies [29–31]. Our results provide support for the hypothesis that neural activity in the posterior fusiform gyrus was modulated by spatial attention over the latency range 90–130 ms, and it is consistent with the combined ERP and blood-flow neuroimaging evidence [30].

4. Discussions

ISM may be a good choice for really focal neural activity of the brain. DSM, in the other hand, may be appropriate to other cases, such as complex cognitive processes and widespread epileptic discharges. In this work, we present GSM, consisting of a "group" of sources, being determined by the center of the "group" and the support range of a Gauss distribution to combine the advantages of ISM and DSM. Based on GSM, we developed GIA to tackle the EEG inverse problem. The above simulation tests show that GIA can localize both isolated and extended sources robustly. In addition, GIA was applied to spatial attention task data measured in a real condition and successfully reconstructed sources on contralateral occipital cortices, which is consistent with the psychological assumption [30].

In literature [23], it was proved that FOCUSS is absolutely convergent with at least a quadratic rate of convergence. In GIA, we adopt the same steps as FOCUSS, except that the search space is smoothed by Gaussian function with the flexible support range, so the behavior of the searching space is the only factor that may affect the convergence of GIA. Indeed, using Gaussian function distribution for each area, the search space may become larger than that of the previous step, which may cause the process failed to converge. To avoid this case, as described in Section 2.6, we stop the "GSM process", the solution space iteration, and continue the iterative calculation along the basic FOCUSS in a fixed solution space which is guaranteed to converge. Apparently, in this way, GIA is always convergent.

We highlight the smoothing process of GIA. In contrast with FOCUSS, which iteratively weights the solution space to reinforce or weaken regions of the solution space where the source strengths are relatively strong or weak, respectively. And in this process, some fake sources due to measurement noise are not easy to be inhibited; some spurious peaks may exist in the final result. In GIA, the Gaussian function effectively filters the spiky spurious sources and imposes a relatively weak weighting on the corresponding nodes in the following iterations. This smoothing process gives more opportunity to avoid falling in local minima, which is similar to the simulated annealing (SA) optimization [20] in finding the global minimum.

In this work, GIA was evaluated first by various computer simulations, and the result indicates that GIA can improve the localization ability when compared with FOCUSS and LORETA. The improvement was due to the using of a Gaussian kernel to reduce spurious sources, which may be problematic for the FOCUSS algorithm [12] when strong noise existed in the EEG recordings. The support range parameter of the Gaussian function σ directly affected those GIA performances such as elimination of spurious sources and the spatial resolution, a larger one avails for the removing of noise and a small one corresponds to a high (local) spatial solution. The dynamic adjustment of σ provides the iteration a stable process from an initial smooth filter for removing spurious sources to a final relative focal localization. When the actual source is ISM, the final smoothness of the smoothing operator is almost zero, and GIA is the same as FOCUSS. In case of an extended source distribution, the support range of the smoothing kernel will be spread widely, and GIA was likely to give a blurred solution, just like LORETA. The smart adjustment of σ makes GIA a flexible integration of FOCUSS and LORETA.

The above simulation studies indicate that GIA is able to recover various sources, isolated point sources or distributed sources. GIA

Table 2
Evaluation indexes for extended source under noise of $NSR = 0.15$.

Index	GSM centered at (−15, −75, 15) (mm)				DSM centered at (60, −25, 35) (mm)			
	Simu.	LORETA	FOCUSS	GIA	Simu.	LORETA	FOCUSS	GIA
$E_{localization}$ (mm)	0	3.1751	2.0734	0.3208	0	5.4003	4.2857	0
$E_{average}$	0	0.8937	0.4629	0.3121	0	0.927	0.8731	0.019
NBI	0.9339	0.8847	0.8744	0.9613	1	0.9825	0	0.98

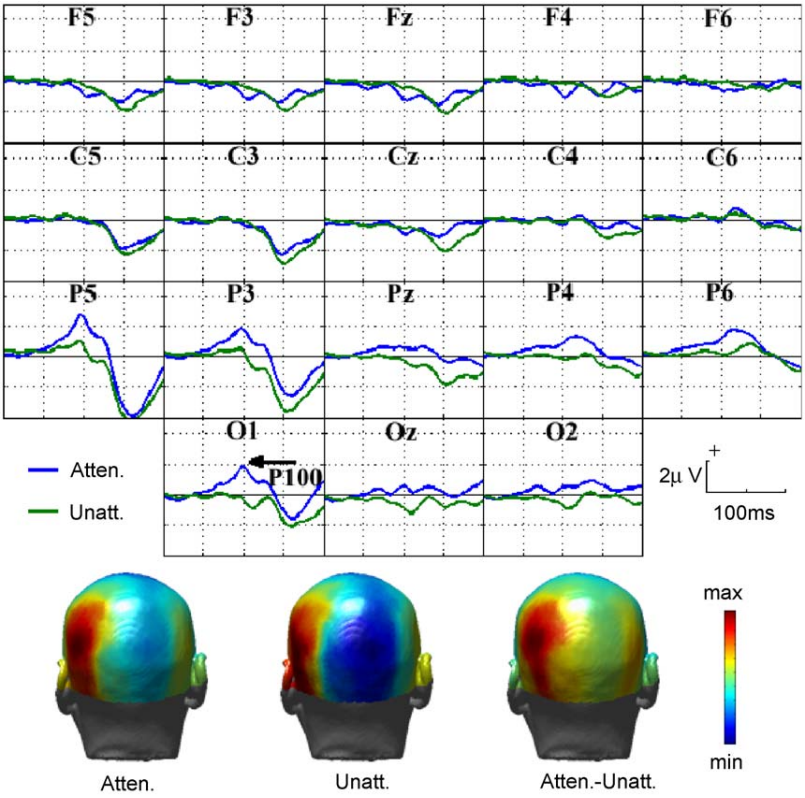

Fig. 7. Visual evoked potential collected in a spatial attention task. The stimulus is in the right visual field. Upper part: Averaged time series between 0 and 200 ms after stimulus onset, the blue curves stand for attentive state (atten.), and the green curves stand for un-attentive state (unatt.). Lower part: Averaged scalp patterns at 96 ms and difference of attentive and un-attentive pattern (atten.–unatt.). (For interpretation of the references to color in this figure legend, the reader is referred to the web version of this article.)

improved the localization ability by iteratively reducing possible spurious sources in a Gaussian smoothing strategy. The combination of GSM into the weighted minimum norm solution (WMNS) can force the solution to robustly converge to a reasonable distribution with desired localization and energy error. Furthermore, the solution of GIA is Gaussian distributed in the brain area, which might be physiologically consistent with the actual brain activations with large number of neurons.

In ISM, the widely adopted algorithms are various optimization approaches; In DSM, linear approach (such as LORETA) and iterative linear approach (such as FOCUSS) is the usually accepted realization. For GSM, though an iterative linear approach is proposed in this paper, it can be realized by optimization approach, too. And this fact again shows that GSM is an advantage integration of ISM and DSM, and that is why our simulation studies indicate GIA is able to recover various sources from isolated points to distributed ones.

In current work, we adopted an isotropic Gaussian function in the three orthogonal directions. For actual neural activities, it may be anisotropic, thus an anisotropic GSM may be a better model of the actual distributed sources. For anisotropic GSM, the current scalar σ will be replaced by a vector σ. In general, the anisotropy may be assumed by possible anatomic information, or determined by applying Eq. (9) for the three orthogonal directions separately.

In summary, GSM and GIA improved the localization ability by reducing spurious sources. The validation of GIA for EEG source imaging is confirmed by the above simulation tests and a real data test. GIA appears to have small localization and energy error, and it is robust to noisy data. The combination of GSM into WMNS can force the solution to converge to the actual source. Furthermore, in our practice, GIA is efficient, as only several iteration steps are needed for the algorithm to converge.

The role of study sponsors

Lei: In the study design, in the collection, analysis and interpretation of data; in the writing of the manuscript.

Xu and Chen: In the analysis and interpretation of data.

Yao: In the analysis and interpretation of data; in the writing of the manuscript; in the decision to submit the manuscript for publication.

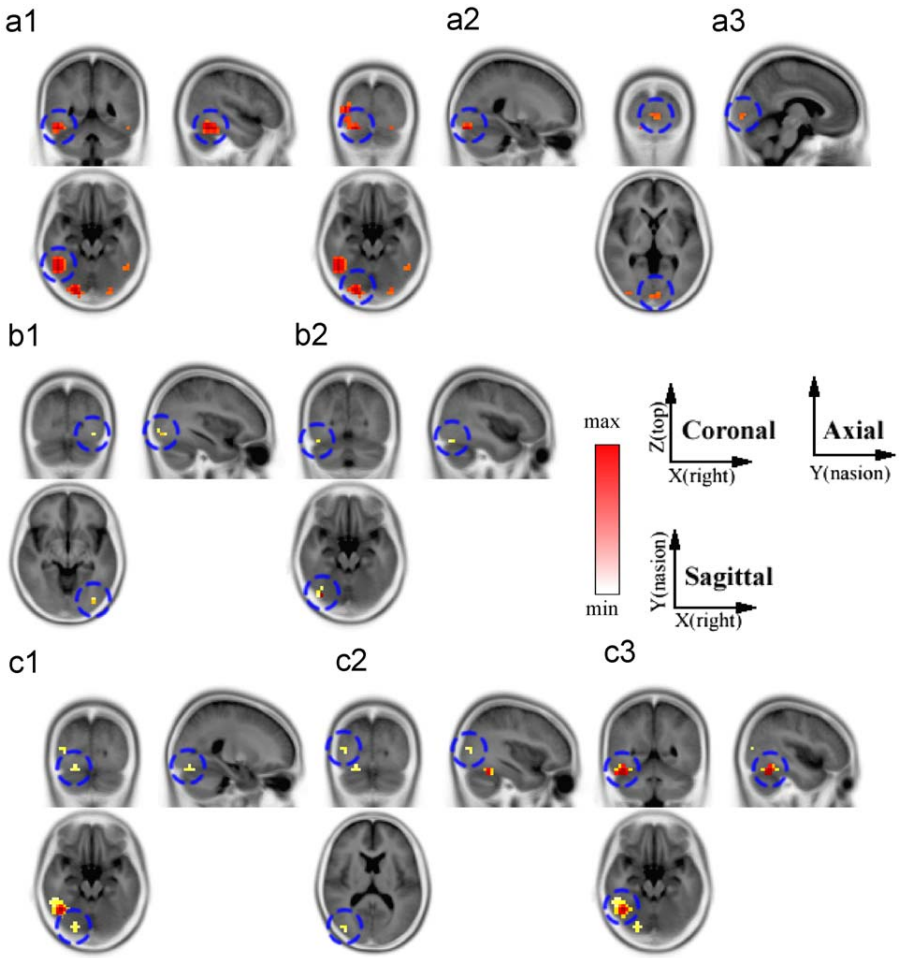

Fig. 8. The activations of attended case detected by these three methods: (a) LORETA, (a.1) left temporal inferior, (a.2) left fusiform gyrus, (a.3) right calcarine cuneus; (b) FOCUSS, (b.1) right inferior occipital, (b.2) left fusiform gyrus; and (c) GIA, (c.1) left occipital fusiform gyrus, (c.2) left middle occipital gyrus, (c.3) left temporal fusiform gyrus.

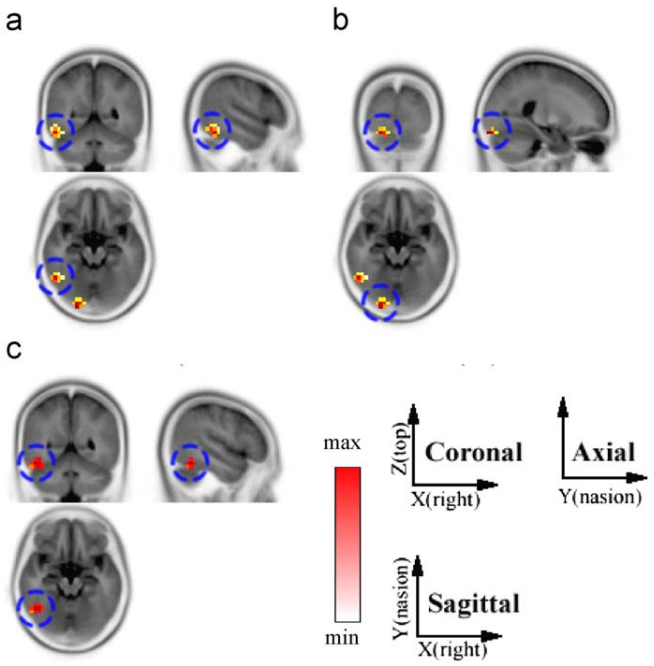

Fig. 9. The activations of the difference wave detected by GIA. (a) unattented, (a.1) left temporal fusiform gyrus, (a.2) left inferior occipital gyrus and (b) attented-unattented, left temporal fusiform gyrus.

Conflict of interest statement

The authors have declared that no competing interests exist.

Acknowledgments

This work was supported by NSFC (#30525030, #60736029 and #60701015) and the 863 Project 2009AA02Z301. Thanks to Dr. X.Y. Ao and Prof. L. Chen for real data collection.

References

[1] E.J. Speckmann, C.E. Elger, Introduction to the Neurophysiological Basis of the EEG and DC Potentials, in: E. Neidermeyer, F. Lopes da Silva (Eds.), Electroencephalography: Basic Principles, Clinical Applications and Related Fields, fifth ed., Lippincott Williams and Wilkins, New York, 2005.
[2] G. Buzsaki, R.D. Traub, T.A. Pedley, The cellular basis of EEG activity, in: J.S. Ebersole, T.A. Pedley (Eds.), Current Practice of Clinical Electroencephalography, third ed., Lippincott Williams and Wilkins, Philadelphia, 2003.
[3] P. Gloor, Neuronal generators and the problem of localization in electroencephalography: application of volume-conductor theory to electroencephalography, J. Clin. Neurophysiol. 2 (1985) 327–354.
[4] C.M. Michel, M.M. Murray, G. Lantz, S. Gonzalez, L. Spinelli, R. Grave de Peralta, EEG source imaging, Clin. Neurophysiol. 115 (2004) 2195–2222.
[5] M. Scherg, D. von Cramon, Evoked dipole source potentials of the human auditory cortex, Electroencephalogr. Clin. Neurophysiol. 65 (1986) 344–360.
[6] S. Baillet, J.C. Mosher, M. Leahy, Electromagnetic brain mapping, IEEE Signal Process. Mag. 18 (2001) 14–30.
[7] C. Benar, R.N. Gunn, C. Grova, B. Champagne, J. Gotman, Statistical maps for EEG dipolar source localization, IEEE Trans. Biomed. Eng. 52 (2005) 401–413.

[8] M.S. Hämäläinen, R.J. Ilmoniemi, Interpreting measured magnetic fields of the brain: estimates of current distributions. Technical Report, Helsinki University of Technology Helsinki Finland, 1984, TKK-F-A559.
[9] F. Babiloni, C. Babiloni, F. Carducci, G.L. Romani, P.M. Rossini, L.M. Angelone, F. Cincotti, Multimodal integration of high resolution EEG and functional magnetic resonance imaging data: a simulation study, NeuroImage 19 (2003) 1–15.
[10] C. Grova, J. Daunizeau, J.M. Lina, C.G. Bénar, H. Benali, J. Gotman, Evaluation of EEG localization methods using realistic simulations of interictal spikes, Neuroimage 29 (2006) 734–754.
[11] R.D. Pascual-Marqui, C.M. Michel, D. Lehmann, Low resolution electromagnetic tomography: a new method for localizing electrical activity in the brain, Int. J. Psychophysiol. 18 (1994) 49–65.
[12] I.F. Gorodnitsky, J.S. George, B.D. Rao, Neuromagnetic source imaging with FOCUSS: a recursive weighted minimum norm algorithm, Electroencephalogr. Clin. Neurophysiol. 95 (1995) 231–251.
[13] P. Xu, Y. Tian, H. Chen, D. Yao, LP norm iterative sparse solution for EEG source localization, IEEE Trans. Biomed. Eng. 54 (3) (2007) 400–409.
[14] S. Baillet, L. Garnero, A Bayesian, approach to introducing anatomofunctional priors in the EEG/MEG inverse problem, IEEE Trans. Biomed. Eng. 44 (5) (1997) 374–385.
[15] K. Friston, L. Harrison, J. Daunizeau, S. Kiebel, C. Phillips, N. Trujillo-Barreto, R. Henson, G. Flandin, J. Mattout, Multiple sparse priors for the MEG/EEG inverse problem, NeuroImage 39 (2008) 1104–1120.
[16] J.F. Murray, K. Kreutz-Delgado, An improved Focuss-based learning algorithm for solving sparse linear inverse problems, in: IEEE International Conference on Signals, Systems and Computers, vol. 1, 2001, pp. 4–7.
[17] D. Yao, The equivalent source technique and cortical imaging, Electroencephalogr. Clin. Neurophysiol. 98 (1996) 478–483.
[18] P. Xu, Y. Tian, X. Lei, X. Hu, D. Yao, Equivalent charge source model based iterative maximum neighbor weight for sparse EEG source localization, Ann. Biomed. Eng. 36 (12) (2008) 2051–2067.
[19] A. El Badia, T. Ha-Duong, An inverse source problem in potential analysis, Inverse Prob. 16 (2000) 651–663.
[20] K. Uutela, M. Hamalainen, R. Salmelin, Global optimization in the localization of neuromagnetic sources, IEEE Trans. Biomed. Eng. 45 (1998) 716–723.
[21] D. Yao, B. He, A self-coherence enhancement algorithm and its application to enhancing 3D source estimation from EEGs, Ann. Biomed. Eng. 29 (11) (2001) 1019–1027.
[22] H.S. Liu, X.R. Gao, P.H. Schimpf, F.S. Yang, S.K. Gao, A recursive algorithm for the three dimensional imaging of brain electric activity: shrinking LORETA-FOCUSS, IEEE Trans. Biomed. Eng. 51 (2004) 1794–1802.
[23] I.F. Gorodnitsky, B.D. Rao, Sparse signal reconstruction from limited data using FOCUSS: a re-weighted minimum norm algorithm, IEEE Trans. Signal Process. 45 (1997) 600–616.
[24] D. Yao, High-resolution EEG mapping: a radial-basis function based approach to the scalp Laplacian estimate, Clin. Neurophysiol. 113 (2002) 956–967.
[25] P.L. Nunez, R. Srinivasan, Electric Fields of the Brain: The Neurophysics of EEG, second ed., Oxford University Press, New York, 2006 p. 251.
[26] H.P. Op de Beeck, J. Haushofer, N.G. Kanwisher, Interpreting fMRI data: maps, modules and dimensions, Nat. Rev. Neurosci. 9 (2008) 123–135.
[27] P. Olejniczak, Neurophysiologic basis of EEG, J. Clin. Neurophysiol. 23 (2006) 186–189.
[28] J. Talairach, P. Tournoux, Co-planar Stereotaxic Atlas of the Human Brain, Thieme, Stuttgart, Germany, 1988.
[29] M.G. Woldorff, P.T. Fox, M. Matzke, J.L. Lancaster, S. Veeraswamy, F. Zamarripa, M. Seabolt, T. Glass, J.H. Gao, C.C. Martin, P. Jerabek, Retinotopic organization of early visual spatial attention effects as revealed by PET an ERPs, Hum. Brain Mapping 5 (1997) 280–286.
[30] S.A. Hillyard, L. Anllo-Vento, Event-related brain potentials in the study of visual selective attention, Proc. Natl. Acad. Sci. USA 95 (1998) 781–787.
[31] D. Yao, Computation for the implicit components of ERP in attention, Brain Topogr. 16 (1) (2003) 65–70.
[32] X.Y. Ao, S.L. Fan, X. He, L. Chen, ERP studies of spatial selective attention to upper and lower visual field, Acta. Biophys. Sin. 16 (1) (2000) 73–80.

Xu Lei was born in Chongqing, China, in 1982. He received the B.S. degree in Information and Computational Science from University of Electronic Science and Technology of China (UESTC), Chengdu, in 2005. He is now pursuing the Ph.D. degree in Biomedical Engineering with UESTC. His research interests include EEG classification, EEG inverse problem, and EEG/fMRI fusion.

Peng Xu was born in Yunnan Province, China, in 1977. He received the B.S., M.S., and Ph.D. degree from UESTC, in 1999, 2002, and 2006 in Biomedical Engineering. His research interest is brain computer interface.

Antao Chen was born in Sichuan Province, China, in 1973. He received the Ph.D. degree from Southwest University in 2005. His research interests include data mining.

De-Zhong Yao was born in Chongqing, China, 1965. He received the Ph.D. degree in Applied Geophysics from the Chengdu University of Technology, Chengdu, China, in 1991, and completed his Postdoctoral Fellowship in Electromagnetic Field with UESTC in 1993. He has been a Faculty member since 1993, a Professor since 1995, and the Dean of the School of Life Science and Technology, UESTC since 2001. He was a Visiting Scholar with the University of Illinois at Chicago from September 1997 to August 1998, and a Visiting Professor with the McMaster University Canada from November 2000 to May 2001 and with the Aalborg University, Denmark, from November 2003 to February 2004. He has published more than 60 peer reviewed papers in international journals and conferences. His current research interests include EEG and fMRI with their applications in cognitive science and neurological problems.